

WILDFIRE INFLUENCE ON SNOW ENERGY BALANCE FROM 22 YEARS OF MODIS LAND SURFACE ALBEDO

Jillian M. Gayler^{1*} and S. McKenzie Skiles¹

¹ *University of Utah, Salt Lake City, UT*

ABSTRACT: A changing climate increasingly impacts snow in the western US, from altered precipitation patterns to heightened wildfire potential in the seasonal snow zone. Fire in the seasonal snow zone removes forest canopy, exposing the underlying snow cover and modifying snow accumulation and melt periods, subsequently altering the surface energy balance. Scientific understanding of impacts from wildfire on the snowpack and surface energy balance is limited, restricting the ability to synthesize how altered surface energy fluxes impact snowpack dynamics. This study analyses 22 years of remotely sensed land surface albedo (LSA) in the seasonal snow zone to deepen scientific understanding of wildfire impacts on snow. In a high elevation, high severity fire followed by an above average snowpack, average winter LSA was 23.7% higher than the unburned area LSA (p-value: 0.002) in the first four years following fire, potentially contributing to a localized temperature cooling effect. As wildfires increase in frequency, elevation, and intensity in the mountain west, considering their impact on the surface energy balance within the broader context of snow hydrology and avalanche hazard becomes increasingly crucial.

KEYWORDS: Snow hydrology, wildfire, remote sensing

1. INTRODUCTION

Snowpack dynamics and wildfires are increasingly becoming inextricably linked as a changing climate leads to longer drought periods and higher temperatures. Snowpacks are predicted to continue to decline throughout this century, with significant impacts in the seasonal snow zone of the Western US, (Gergel et al., 2017; Mote et al., 2018). The area of overlap between fire hazards and the seasonal snow zone is growing (Alizadeh et al., 2021; Gleason et al., 2019; Hatchett, 2021) and we are seeing wildfires burn more frequently and intensely at higher elevations. Wildfires in the seasonal snow zone remove forest canopy, exposing the underlying ground cover and modifying the snow accumulation and ablation periods; deposit black carbon and charred woody debris on the snow surface; alter longwave emission from vegetation; and increase turbulent fluxes by allowing more wind transport and potentially changing the air and ground temperature (Liu et al., 2005; Boon, 2009; Burles and Boon, 2011; Winkler, 2011; Gleason et al., 2013; Gleason et al., 2016; Uecker et al., 2020). Each of these consequences impacts the surface energy balance, with implications for the energy available for melt in the snowpack and snowpack metamorphism.

The land surface is an important component of earth system models. The land surface energy balance in winter seasonal snow zones is strongly associated with broadband albedo, the ratio of reflected to incoming solar radiation (0.3-5.0 μm). A shift in the land surface albedo (LSA) changes the amount of solar radiation absorbed by the earth ('radiative forcing'). If the energy input into the

earth system increases (e.g. due to decreasing LSA) then the associated temperature response is to increase, due to greater radiation emittance required to maintain equilibrium in the earth's energy balance. A decrease in LSA will have the opposite effect – higher surface albedo leads to negative radiative forcing and can cause landscapes to exert a cooling effect on climate, relative to landscapes with a lower surface albedo.

Forests, even with snow on the ground under the canopy, can heat the atmospheric boundary layer due to low albedo (Douveille & Royer, 1996). Snow's high albedo (0.9-0.95 for new snow) can increase LSA for forested areas from 0.10-0.13 in snow-off conditions to 0.15-0.24 in snow-on conditions, depending on presence of canopy snow (Wiscombe and Warren, 1980; Barnes and Roy, 2010, Rother et al., 2022). Furthermore, LSA has been shown to increase in burned areas relative to unburned areas in Wyoming (Gersh et al., 2022). As a response to increases in LSA over 5+ years post-fire, surface temperatures have been shown to decrease relative to pre-fire conditions (Liu et al., 2019). The snowpack response to wildfire depends on both this climate feedback as well as increased solar radiation incident at the snow surface.

The LSA response to a transition from snow-hiding (pre-burn) to snow-revealing (post-burn) landscapes in the Sierra Nevada, CA has not been quantified to date. Similarly, the radiative forcing and associated temperature feedbacks due to LSA changes from fire in the seasonal snow zone are not fully understood. This work seeks to quantify changes in LSA in the Sierra Nevada sea-

sonal snow zone due to wildfires in order to understand the regional climate feedbacks and impacts on snow energy balance and internal snow-pack processes. We apply remotely sensed LSA and snow cover products from Moderate Resolution Imaging Spectrometer (MODIS) imagery to quantify post-fire LSA evaluate the magnitude of change in LSA and surface radiative forcing in the Sierra Nevada seasonal snow zone.

2. STUDY AREA AND DATA

2.1 Study Area

The Sierra Nevada extends over 450 miles between the latitudes of 40.5° N and 35.6° N. The region is dominated by high interannual precipitation and temperature variability, with 60-80% of precipitation falling as snow in the winter. The area considered in analysis consists of the seasonal snow zone on the western slope of the Sierra Nevada (Figure 1), an area spanning 5,000-8,000 feet in elevation. The seasonal snow zone is defined, for the purpose of this study, as pixels with greater than 50% snow cover between January 1 - April 1 over the MODIS record (2001-2022).

We analyzed two fires that burned into the seasonal snow zone: the 2018 Donnell Fire, which burned primarily at high severity, was almost entirely contained within the seasonal snow zone, and was followed by a high snow year; and the 2013 Rim Fire, which burned primarily at low severity at lower elevation and was followed by a low snow year (Table 1).

2.2 Data

The snow fraction and LSA datasets used in this analysis are sourced from the MODIS sensor aboard the NASA satellite Terra. The MODIS sensor measures reflected solar radiation from the earth's surface every 1-2 days. Spatial resolution in the land bands is 500 meters. The MODIS LSA product, MCD43A3 (Schaaf et al., 2015), provides 16-day averaged reflectance measurements in the visible, near-infrared, and broadband ranges for directional hemispherical reflectance (black-sky albedo [BSA]) and bihemispherical reflectance (white-sky albedo [WSA]). The actual bidirectional reflectance albedo ("blue-sky" albedo) is a ratio of BSA and WSA; what we report as LSA is a simple 1:1 ratio of BSA to WSA (French et al., 2016).

* *Corresponding author address:*

Jillian M. Gayler, University of Utah Snow HydRO Lab, Salt Lake City, UT 84101; email: jillian.gayler@utah.edu

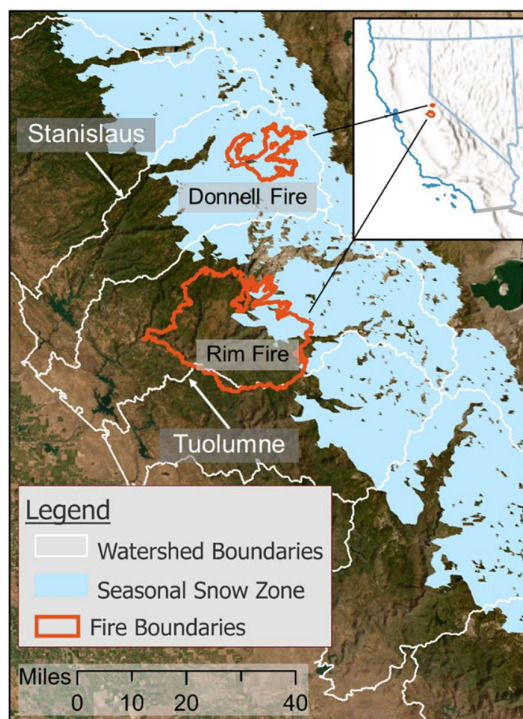


Figure 1. The Donnell Fire and Rim Fire boundaries shown in orange, watershed boundaries shown in white, and the seasonal snow zone shown in blue.

The MODIS Snow Cover and Grain Size (MODSCAG) algorithm uses surface reflectance data from the MODIS product MOD09GA to retrieve snow properties using spectral mixture analysis (SMA), including the fraction of each pixel covered by snow (Painter et al., 2009). The SMA workflow is based on a set of linear equations that solve for subpixel fraction of clean snow, shade, vegetation, rock, and other surface covers. The snow-covered fraction (SCF) retrieval quantifies snow cover in both open and forested areas, using interpolation to calculate SCF under the forest canopy (Rittger, et al., 2020). For this analysis, we used a spatially and temporally complete version of MODSCAG where data gaps (e.g. from cloud obscuration) are filled to produce a daily product (Rittger et al., 2021).

Data on burn area and severity were obtained from Monitoring Trends in Burn Severity (MTBS), an interagency program managed by the U.S. Geological Survey Center for Earth Resources Observation and Science (EROS) and the USDA Forest Service (USFS) Geospatial Technology and Applications Center (GTAC) (Eidenshink et al., 2007). MTBS products leverage Landsat 30-meter spatial resolution data and data from similar sensors to generate burn severity maps, including fire boundaries and mosaics of burn severity within. Each pixel is designated with one of

Table 1. Characteristics of burned pixels in the SSZ from the two Sierra Nevada wildfires analyzed in this study. Burn area refers to the entire fire extents; all other characteristics are representative of only the overlapping area between fire scar and seasonal snow zone.

Fire	Watershed	Ignition Year	Total Burn Area (ac)	Average Elev. (ft)	Primary Burn Severity	2011 Tree Cover (%)
Donnell	Stanislaus	2018	36,200	7,000	High	49
Rim	Tuolumne	2013	257,100	5,600	Low	30

five classifications: unburned, unburned to low, low, moderate, and high. We resampled the MTBS data to MODIS resolution using a modal resampling method.

Downward shortwave radiation (DSR) data was obtained from the NASA GeoNEX DSR/PAR product, which uses top of atmosphere (TOA) reflectance to generate a physical-based look-up table for hourly at-surface DSR at 1 km resolution (Li et al., 2022). We resampled the data into monthly values at MODIS spatial resolution.

Tree cover data were obtained from the USFS GTAC and FIA Tree Canopy Cover (TCC) dataset, which contains percent tree canopy estimates for each 30-meter pixel across the continental U.S as part of the NLCD (Coulston et al., 2012). We used the TCC dataset from 2011 as it maps TCC prior to the occurrence of the analyzed fires. The tree cover dataset was resampled to MODIS resolution using a bilinear resampling method.

Snow water equivalent data was gathered from the California Cooperative Snow Survey (CCSS) sensors. The three sensors closest to each fire scar/seasonal snow zone overlap were used in analysis.

3. METHODS

To quantify changes in LSA from wildfire, LSA was analyzed under the following three conditions: pre-fire, post-fire in the burn scar (LSA_b) and post-fire outside the burn scar (LSA_u). All data was masked to MODIS pixels within the seasonal snow zone. The burned area was masked to only high burn severity pixels. The unburned pixels selected for comparison were within the same watershed boundary, had greater than 40% tree cover, and had not been burned by any other fire within the previous 10 years. The pre-fire historical average LSA was calculated by averaging LSA in all high severity burned pixels within the fire scar for each calendar month over the years leading up to the ignition date.

We analyzed changes in LSA at the fire scar-scale in two ways: first, the difference between

LSA_b to LSA_u , and second, the difference between the pre-fire historical average LSA to LSA_b . Comparisons of each were made by calculating the mean LSA values for winter (December through February) and spring (March through May). We then analyzed a time series comparison between pre-fire monthly average LSA values, LSA_u , and LSA_b in the first four years following each fire.

Changes in monthly LSA were then used in conjunction with DSR to calculate the albedo-induced surface radiative forcing. We calculated radiative forcing using the equation:

$$RF = (LSA_b - LSA_u) * DSR$$

where RF represents the surface radiative forcing and LSA_b and LSA_u represent the LSA for burned and unburned areas, respectively. We used monthly DSR values, averaged over the available data record from January 2018 through December 2021 (Liu et al., 2005), and used an average monthly LSA_b and LSA_u from the first four years post-fire to determine surface radiative forcing for high burn severity areas.

4. RESULTS

4.1 Wildfire Trends in Seasonal Snow Zone

The MTBS records starting in 1984 show that over 250 wildfires have burned in the Sierra Nevada. Over this record, fires have burned larger areas and at higher elevations, increasingly impacting the seasonal snow zone. Trends in annual highest burn elevation and annual maximum fire size exhibit interannual variability, but both show clear increasing trends over time (Figure 2). Both increasing trends were significant at the 5% level using a Mann-Kendall trend test (elevation p -value: 0.01, size p -value: 0.001).

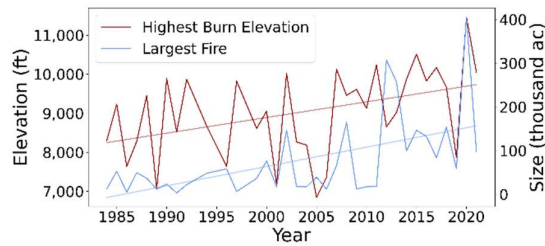


Figure 2. Annual time series of the highest elevation fire and the largest fire over the MTBS record. Both trends show a significant increase.

4.2 Changes in LSA in a High Elevation, High Severity Fire

In the Donnell Fire scar, LSA in the burned area was consistently higher than LSA in forested pixels outside the burn area, an impact that lasted for years following the fire. Sentinel-2 L2A RGB images over the Donnell Fire from a snow-off date show that impacts from the Donnell fire are visibly evident; the lack of vegetation in the fire scar shows up as a stark difference from the darker, vegetated unburned area (Figure 3). Corresponding MCD43A3 LSA images reveal that the LSA values show the same characteristic. In the snow-on image, the fire scar is less evident. However, the burn area pixels have a higher LSA than the unburned forested area, and a lower LSA than the nearby snow-covered, low tree cover pixels (Table 2).

Table 2. Land cover characteristics for each of the boxes shown in Figure 4.3. Tree cover data is from pre-fire conditions; all other variables represent characteristics on the shown date.

	Burn Classification	2011 Tree Cover (%)	SCF (%)	LSA
A1	Unburned	50.5	0.0	0.10
A2	Burned – High Severity	47.5	0.0	0.15
A3	Unburned	18.0	0.0	0.20
M1	Unburned	50.5	92.8	0.30
M2	Burned – High Severity	47.5	87.6	0.58
M3	Unburned	18.0	94.3	0.75

4.3 Comparing Two Extremes

Change in LSA following fire varied considerably between the Donnell Fire and the Rim Fire (Figure 4). The Donnell Fire showed a significant increase in winter and spring LSA. In the winter following the Donnell fire, the average LSA_b was

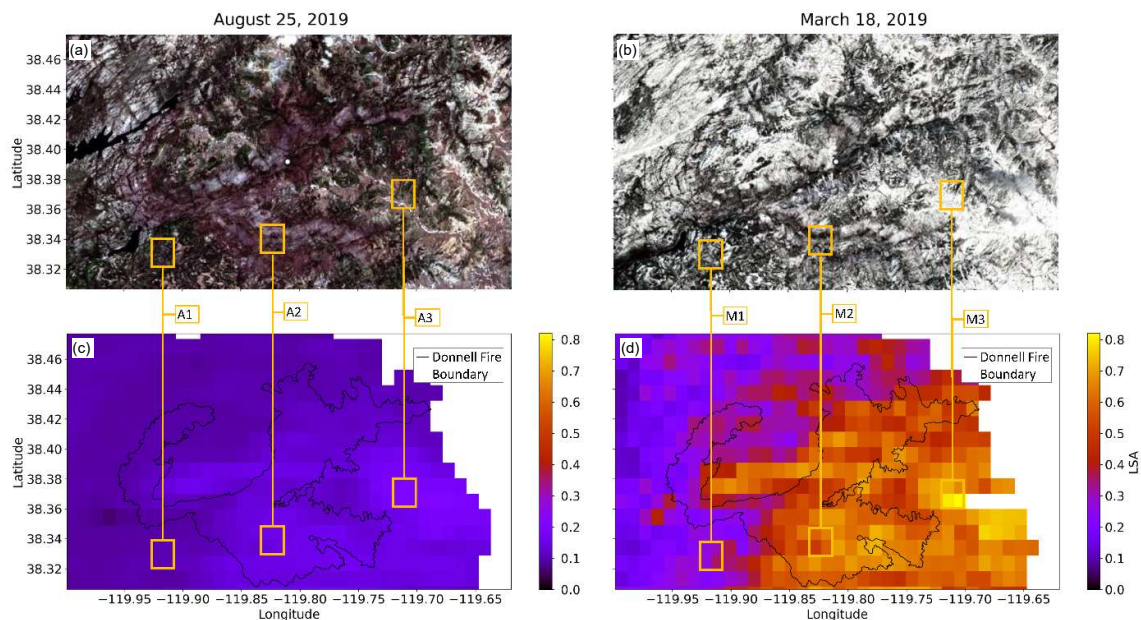


Figure 3. Sentinel-2 L2A RGB images of the Donnell Fire in (a) snow-off and (b) snow-on conditions and the MCD43A3 LSA mosaic shown for the same (c) snow-off and (d) snow-on days, with the Donnell Fire outlined. Corresponding areas are shown in connecting boxes. The MCD43A3 images are 16-day averages centered on the date of the Sentinel-2 L2A overpass. Characteristics for each labeled box are summarized in Table 2 for reference.

0.47 (sd = 0.13) and the average LSA_u in forested pixels was 0.24 (sd = 0.12), a ~96% increase. In the spring the average LSA_b was 0.45 (sd = 0.10) and the average forested LSA_u was 0.19 (ds = 0.11), a ~137% increase. The trend of Donnell Fire LSA_b being significantly higher than the LSA_u continued in the next three years and, while the LSA_u varied little from the historical average or showed an average negative anomaly, the LSA_b was consistently higher than the historical average by 0.14-0.25. In contrast, in the winter following the 2013 Rim fire, the average LSA_b was 0.12 (sd = 0.05) and the average LSA_u in forested pixels was 0.11 (sd = 0.06), a ~5% increase. In the spring, the average LSA_b was 0.09 (sd = 0.07) and the average forested LSA_u was 0.11 (ds = 0.06), a change of ~-18%. In the four years following the Rim Fire, LSA_b was consistently lower than LSA_u in both winter and spring.

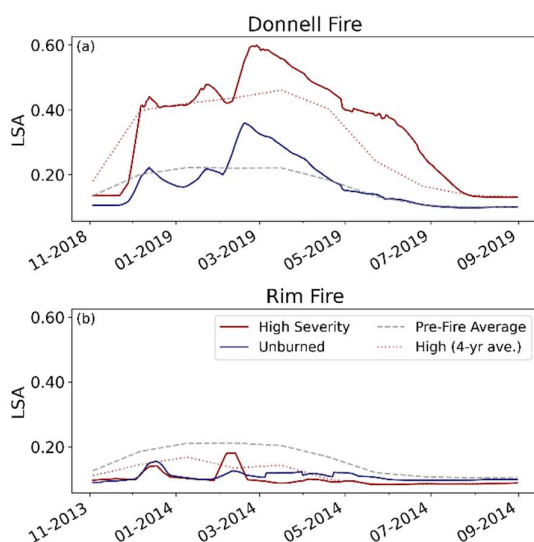


Figure 4. A time series of LSA_b, LSA_u, and the historical average LSA.

The differences between the two fire scar LSA responses is likely due, in part, to the snow conditions following each fire. The Donnell Fire was preceded by higher-than average SWE and SCF, while the Rim fire was followed by extremely low snow conditions (Figure 5). Differences in mean SWE and SCF were significant at the 1% significance level using a two-sample t-test.

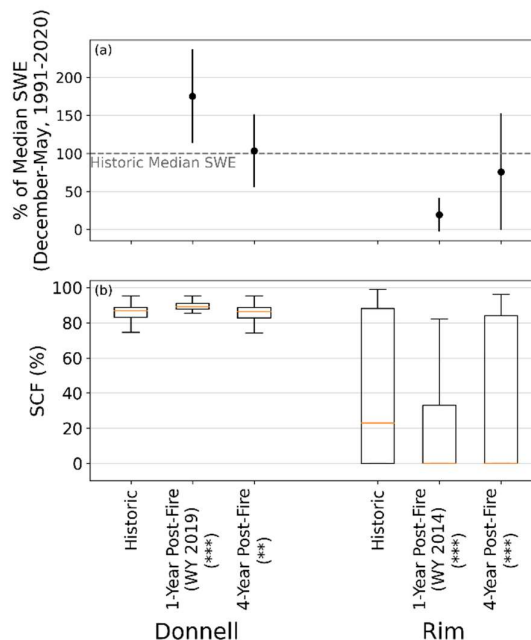


Figure 5. Comparisons of post-fire snow characteristics compared to historical values. Figure 5a shows the December-May % of 1991-2020 median SWE for one year post-fire and four years post-fire, with error bars representing 1 standard deviation. Figure 5b shows the December-May boxplots for historic, 1-year post-fire, and averaged 4-years post-fire SCF. (** = p value < 0.01; *** = p value < 0.001 from Welch's t-test.)

4.4 Surface Radiative Forcing

Consistently negative surface radiative forcing values in the Donnell Fire scar revealed that more solar radiation was reflected by the landscape post-fire relative to pre-fire. In the first year following the Donnell Fire, this effect was most intense in the late spring into summer (average RF = -60.0 Wm⁻²), when snow influence on LSA persisted in the burned area past the unburned area, and least intense in early to mid-winter (average RF = -29.1 Wm⁻²) (Figure 6), when solar zenith angles are high, and both burned and unburned landscapes were more likely to be blanketed in snow. The 4-year post-fire average radiative forcing due to the Donnell Fire shows the largest RF values shifting earlier in the year to March and April. Radiative forcing values of 0.5 and -4.4 Wm⁻² preceded the Rim Fire in the first winter and spring post-fire, respectively. In the four years following the Rim Fire, the radiative forcing trended increasingly positive over the winter, when darkened, charred forests and low snow cover resulted in lower LSA_b, then minimized in the late spring into summer.

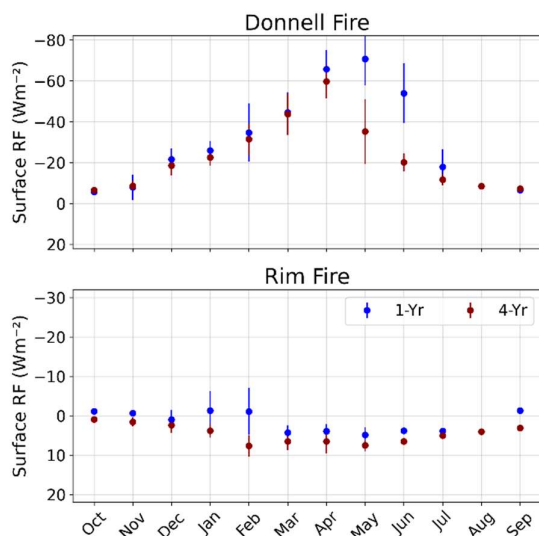


Figure 6. Monthly RF values for 1 year post-fire and averaged over 4 years post-fire.

5. DISCUSSION

Sierra Nevada wildfires have increased in size, intensity, and elevation over the MTBS record and are increasingly impacting the seasonal snow zone (Alizadeh et al., 2021). By removing forest canopy, they shift landscapes from snow-hiding to snow-revealing, altering the surface energy balance. The degree to which LSA responded to fire depended, in part, on snow cover after the fire occurred. The Donnell Fire, a high-elevation, high-burn severity fire followed by a significantly larger-than-average snow year, showed that LSA can increase from 0.19-0.24 to 0.45-0.47 after a fire. In contrast, post-fire low-snow conditions after the relatively low-elevation Rim Fire led to decreases in LSA_b with respect to LSA_u and historical LSA, suggesting that post-fire landscapes in low-snow conditions are likely dominated by fire-related landscape darkening.

The radiative forcing associated with change in vegetation cover and subsequent snow exposure varied considerably between the two fire conditions. We found that in the year after the Donnell Fire, changes in LSA led to an average winter and spring radiative forcing value of -60.0 Wm⁻² and -29.1 Wm⁻², respectively. The Rim Fire showed a minimal change in absorption of downward shortwave radiation, with average winter and spring radiative forcing values of 0.5 Wm⁻² and -4.36 Wm⁻², respectively. As low-snow years continued after the Rim Fire, winter radiative forcing grew increasingly positive. The contrasting responses from two different fire scars indicate that post-fire radiative forcing is heavily dependent upon snow conditions and adds to the evidence that snow cover plays a major role in the surface energy balance.

Previous studies have shown that a change in winter LSA due to fire can contribute to localized temperature changes in boreal forests (Liu et al., 2019; Randerson et al., 2006). Further work is needed to quantify temperature responses to radiative forcing caused by wildfire in the seasonal snow zone. These preliminary results suggest that wildfire may lead to a positive feedback loop based on snow conditions – if a large snow year follows a wildfire, then the snow will contribute to negative radiative forcing (the landscape will reflect more solar radiation) and the burned landscape may be cooler than in nearby unburned forested areas. On the contrary, if a low-snow year follows a wildfire, then the winter/spring LSA may be dominated by charred forests, leading to positive radiative forcing values and potentially higher temperatures. However, post-fire snowpacks are also subject to increased solar radiation incident at the snow surface, adding more uncertainty to internal snowpack processes. The impacts of these changes have yet to be quantified, but are becoming increasingly relevant as wildfire frequency and elevation, as well as interannual variability in winter snowpacks, are predicted to increase (Alizadeh et al., 2021; Gergel et al., 2017; Hatchett, 2021; Mote et al., 2018).

6. CONCLUSION

Comparing the results of two wildfires in the Sierra Nevada that burned at different elevations with different post-fire snow conditions showed that post-fire LSA response varies considerably between fire scars. The consistently snow-covered Donnell Fire scar indicated that changes in LSA due to wildfire can lead to a significant decrease in absorbed downward shortwave radiation. In contrast, the Rim Fire scar LSA was more likely dominated by charred forests than snow, and thus resulted in an increase in absorbed downward shortwave radiation relative to unburned forested areas. Results indicate that the transition from a snow-hiding to a snow-revealing landscape leads to negative radiative forcing, on the condition that snow is present in the fire scar.

Quantifying energy balance components in the seasonal snow zone has a multitude of benefits, from improvement of climate models to avalanche forecasts and stream runoff forecasts. Relating energy balance changes in burn scars to snowpack processes enables avalanche forecasters, snow hydrologists, and backcountry recreationalists to better understand the state of the snowpack and improve their decision-making accordingly. As the overlap between fire scar area and the seasonal snow zone grows, it becomes increasingly crucial to understand impacts on snowpacks for water resources, ecosystem, and recreational purposes alike.

ACKNOWLEDGEMENTS

This work is funded by the National Science Foundation, CNH-2 Dynamics of Integrated Socio-Environmental Systems Program, Award #2009726. Spatially and temporally complete MODIS snow data is provided by Karl Rittger/Snow Today.

REFERENCES

- Alizadeh, M., Abatzoglou, J., Luce, C., Adamowski, J., Farid, A., & Sadegh, M. (2021). Warming enabled upslope advance in western US forest fires. *Proceedings of the National Academy of Sciences USA*, *118*, e2009717118. doi:10.1073/pnas.2009717118.
- Barnes, C., & Roy, D. (2010). Radiative forcing over the conterminous United States due to contemporary land cover land use change and sensitivity to snow and interannual albedo variability. *Journal of Geophysical Research*, *115*, G04033. doi:10.1029/2010JG001428.
- Boon, S. (2009). Snow ablation energy balance in a dead forest stand. *Hydrological Processes*, *23*, 2600–2610. https://doi.org/10.1002/hyp.7246.
- Burles, K., & Boon, S. (2011). Snowmelt energy balance in a burned forest plot, Crowsnest Pass, Alberta, Canada. *Hydrological Processes*, *25*, 3012–3029. https://doi.org/10.1002/hyp.8067.
- Coulston, J., Moisen, G., Wilson, B., Finco, M., Cohen, W., & Brewer, C. (2012). Modeling percent tree canopy cover: A pilot study. *Photogrammetric Engineering & Remote Sensing*, *78*(7), 715–727. doi:10.14358/PERS.78.7.715.
- Douville, H., Royer, JF. Influence of the temperate and boreal forests on the Northern Hemisphere climate in the Météo-France climate model. *Climate Dynamics* *13*, 57–74 (1996). https://doi.org/10.1007/s003820050153
- Eidenshink, J., Schwind, B., Brewer, K., Zhu, Z., Quayle, B., & Howard, S. (2007). A project for monitoring trends in burn severity. *Fire Ecology*, *3*(1), 3–21. https://doi.org/10.4996/fireecology.0301003.
- French, N., Whitley, M., & Jenkins, L. (2016). Fire disturbance effects on land surface albedo in Alaskan tundra. *Journal of Geophysical Research: Biogeosciences*, *121*(3), 841–854. https://doi.org/10.1002/2015jg003177.
- Gergel, D., Nijssen, B., & Abatzoglou, J. (2017). Effects of climate change on snowpack and fire potential in the western USA. *Climatic Change*, *141*, 287–299. https://doi.org/10.1007/s10584-017-1899-y.
- Gersh, M., Gleason, K., & Surunis, A. (2022). Forest fire effects on landscape snow albedo recovery and decay. *Remote Sensing*, *14*(16), 4079. https://doi.org/10.3390/rs14164079.
- Gleason, K., McConnell, J., Arienzo, M., Chellman, N., & Calvin, W. (2019). Four-fold increase in solar forcing on snow in western U.S. burned forests since 1999. *Nature Communications*, *10*, 2026. doi:10.1038/s41467-019-09935-y.
- Gleason, K. & Nolin, A. (2016). Charred forests accelerate snow albedo decay: Parameterizing the post-fire radiative forcing on snow for three years following fire. *Hydrological Processes*, *30*, 3855–3870. https://doi.org/10.1002/hyp.10897.
- Gleason, K., Nolin, A. & Roth, T. (2013). Charred forests increase snowmelt: Effects of burned woody debris and incoming solar radiation on snow ablation. *Geophysical Research Letters*, *40*, 4654–4661. https://doi.org/10.1002/grl.50896.
- Hatchett, B. (2021). Seasonal and ephemeral snowpacks of the conterminous United States. *Hydrology*, *8*, 32. doi:10.3390/hydrology8010032.
- Li, R., Wang, D., Wang, W., & Nemani, R. (2022). A GeoNEX-based high-spatiotemporal-resolution product of land surface downward shortwave radiation and photosynthetically active radiation. *Earth System Science Data*, *15*, 1419–1436. https://doi.org/10.5194/essd-15-1419-2023.
- Liu, H., Randerson, J., Lindfors, J., & Chapin III, F. (2005). Changes in the surface energy budget after fire in boreal ecosystems of interior Alaska: An annual perspective. *Journal of Geophysical Research*, *110*, D13101. doi:10.1029/2004JD005158.
- Liu, Z., Ballantyne, A.P. & Cooper, L.A. Biophysical feedback of global forest fires on surface temperature. *Nature Communications*, *10*, 214 (2019). https://doi.org/10.1038/s41467-018-08237-z
- Mote, P., Li, S., Lettenmaier, D., Xiao, M., & Engel, R. (2018). Dramatic declines in snowpack in the western US. *npj Climate and Atmospheric Science*, *1*, 2. https://doi.org/10.1038/s41612-018-0012-1.
- Painter, T., Rittger, K., McKenzie, C., Slaughter, P., Davis, R., & Dozier, J. (2009). Retrieval of subpixel snow covered area, grain size, and albedo from MODIS. *Remote Sensing of Environment*, *113*(4), 868–879. https://doi.org/10.1016/j.rse.2009.01.001.
- Randerson, J. T. et al. The impact of boreal forest fire on climate warming. *Science* *314*, 1130–1132 (2006).
- Rittger, K., Raleigh, M., Dozier, J., Hill, A., Lutz, J., & Painter, T. (2020). Canopy adjustment and improved cloud detection for remotely sensed snow cover mapping. *Water Resources Research*, *56*(6). https://doi.org/10.1029/2019wr024914.
- Rittger, K., Bormann, K., Bair, H., Dozier, J., & Painter, T. (2021). Evaluation of VIIRS and MODIS Snow Cover Fraction in High-Mountain Asia Using Landsat 8 OLI. *Front. Remote Sens.* 2:647154. doi: 10.3389/frsen.2021.647154
- Rother, D., De Sales, F., Stow, D., & McFadden, J. (2022). Impacts of burn severity on short-term postfire vegetation recovery, surface albedo, and land surface temperature in California ecoregions. *PLoS One*, *17*(11), e0274428. doi:10.1371/journal.pone.0274428.
- Schaaf, C., Wang, Z. (2021). MODIS/Terra+Aqua BRDF/Albedo Daily L3 Global - 500m V061 [Data set]. NASA EOSDIS Land Processes Distributed Active Archive Center. https://doi.org/10.5067/MODIS/MCD43A3.061.
- Uecker, T., Kaspari, S., Musselman, K., & Skiles, S. (2020). The post-wildfire impact of burn severity and age on black carbon snow deposition and implications for snow water resources, Cascade Range, Washington. *Journal of Hydrometeorology*, *21*(8), 1777–1792. https://doi.org/10.1175/jhm-d-20-0010.1
- Winkler, R. (2011). Changes in snow accumulation and ablation after a fire in south-central British Columbia. *Streamline Watershed Management Bulletin*, *14*, 1–7.
- Wiscombe, W., & Warren, S. (1980). A model for the spectral albedo of snow. I: Pure snow. *Journal of the Atmospheric Sciences*, *37*, 2712–2733. https://doi.org/10.1175/1520-0469(1980)037<2712:AMFTSA>2.0.CO;2.